PhotoniX

RESEARCH Open Access

Producing focused extreme ultraviolet vortex with Fermat-spiral photon sieves

Junyong Zhang[1*†], Huaiyu Cui[2†], Yuanyuan Liu[3,4†], Xiuping Zhang[1], You Li[1], Dongdi Zhao[2], Yongpeng Zhao[2*] and Qiwen Zhan[3,4,5*]

†Junyong Zhang, Huaiyu Cui, and Yuanyuan Liu contributed equally to this work.

*Correspondence: zhangjy829@siom.ac.cn; zhaoyp3@hit.edu.cn; qwzhan@usst.edu.cn

[1] Key Laboratory of High Power Laser and Physics, Shanghai Institute of Optics and Fine Mechanics, Qinghe Road, 201800 Shanghai, China
[2] National Key Laboratory of Science and Technology on Tunable Laser, Harbin Institute of Technology, Xidazhi Road, 150001 Harbin, China
[3] School of Optical-Electrical and Computer Engineering, University of Shanghai for Science and Technology, Jungong Road, 200093 Shanghai, China
[4] Zhangjiang Laboratory, 100, Haike Road, 201204 Shanghai, China
[5] Westlake Institute for Optoelectronics, 311421 Fuyang, Hangzhou, China

Abstract

Extreme ultraviolet (EUV) light is difficult to focus due to strong absorption of most materials. Photon sieves (PS), rather than Fresnel zone plates (FZP), can focus EUV to smaller spot and suppress the higher orders of secondary maxima by several orders of magnitude. The number of pinholes used in PS is far more than that of transparent rings used in FZP, providing a great flexibility to manipulate structured focusing in EUV. In this work we investigate the Fermat-spiral PS to produce focused vortices with different topological charges. Experiment at the wavelength of 46.9 nm is carried out and multi-planar coherent diffractive imaging is used to retrieve the phase map of the focused EUV vortices. These results show the enormous potential of PS for manipulating EUV light. This study not only provides a compact, affordable substitute to focusing vortices where transmissive optics materials are unavailable, but also provides a route of converting various complex light manipulation ranging from visible light to EUV and soft x-ray.

Keywords: Extreme ultraviolet focusing, Orbital angular momentum, Photon sieves, Coherent diffraction imaing

Introduction

Extreme ultraviolet (EUV) radiation has a wavelength ranging from 10 nm to 121 nm, corresponding to photon energies of 124ev to 10.2ev respectively. Shorter wavelength means higher resolution in focusing and imaging. Thus EUV radiation is attractive for high-resolution imaging and nanometer lithography [1]. Meanwhile, EUV radiation has higher photon energies and deeper penetration depths than electrons, allowing for a nano-scale view into intricate three-dimensional structures, which are important for materials science [2, 3], atto-second metrology [4], and semiconductor characterization. Fortunately, a variety of EUV sources, such as high-harmonic generation (HHG) [5], free-electron lasers (FELs) [6], capillary discharge lasers [7, 8] and solid-state EUV source, have been developed during the past few decades, opening up the possibility of light-matter interactions on the nanometer scale by means of structured EUV illumination [9–11]. Unfortunately, focusing and imaging remains challenging due to the strong absorption of most materials in the EUV regime.

Over the past decade, EUV focusing has undergone a transformation, ranging from reflective and refractive optics to concentrators in the form of diffractive devices [12]. Strong absorption makes it difficult to deploy complicated fine refractive lenses under practical conditions. Diffractive elements, by contrast, become more attractive when the incident wavelengths range from EUV radiation to soft X-rays. To date, focused EUV beams have been achieved primarily with a specialized Fresnel zone plate (FZP). Contrarily, photon sieves (PS) perform better than FZP in terms of producing smaller focal spots and suppression of secondary maxima and higher diffraction orders [13]. Following these works, several theoretical and experimental studies were carried out in visible light to determine the parameters of individual nanostructured holes that generate complex structured light fields at a targeted plane.

One of the most relevant structured light beams are those carrying orbital angular momentum (OAM), also known as vortex beams, which are appealing for application such as in quantum optical communications, particle manipulation [14], lithography [15], super-resolution imaging and so on [16]. Recent advances in high harmonic generation (HHG) have been reported to produce OAM beams in the EUV radiation or x-rays [17–20]. Spurred by these exciting technologies, parallel interest in the ability to focus and manipulate the OAM of ultrafast light pulses has also emerged. However, for the same reason, all fields that use EUV radiation are encumbered by handing problems that arise from the strong absorption. Until now, there is a lack of reports on producing EUV radiation focus, let alone focused EUV field carrying complex OAM. The capability of producing focused EUV vortex optical field with arbitrary topological charges may spur promising applications including the inspection of dynamics of nonhomogeneous molecular systems at the nanometric, optical trapping and super-resolution imaging.

Inspired by the prior works in the visible regime [21–27], here we for the first time, to the best of our knowledge, present the Fermat-spiral PS to realize focused vortices with different topological charges. Focusing is critical for a host of applications in imaging and spectroscopy, as well as for enhancing our ability to optically manipulate macro- to nano-scale objects such as particles, molecules, atoms and electrons. The Fermat-spiral PS with focusing vortices was successfully obtained by genetic optimization algorithm [28], and then its focusing properties, including intensity and phase maps, were measured by means of multi-planar phase retrieval algorithm [29]. The results show that for the first two focused vortices with topological charges of -1 and +3 has the full width at half maximum (FWHM) of the dark ring of 260 nm and 742 nm, respectively. They are all in good agreement with the theory. This research offers a solution to the challenging problem encountered with EUV radiation, which is the lack of suitable optical devices for focusing and controlling light fields. We believe the current work is an important step forward for focusing and manipulating extreme short-wave optical fields, which may have great potential for applications in material science and lithography.

Focused EUV vortex with Fermat-spiral PS

To achieve the focused Vortex in EUV, a Fermat-spiral PS serves as the primary optical component that controls the amplitude and phase of the incident EUV light. The implementation of this concept is shown in Fig. 1a. The incident plane wave is

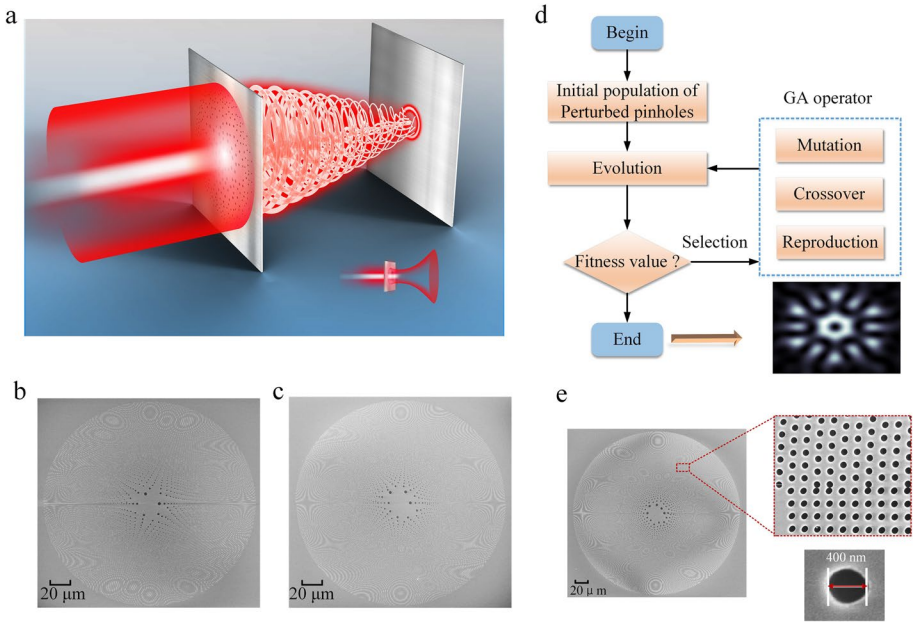

Fig. 1 **a** Sketch of focused OAM. **b** and **c** SEM images of Fermat-spiral PS with topological charge of -1 and +3, respectively. **d** Flowchart of genetic algorithm to optimize Fermat-spiral PS (see (**e**)) so as to produce focused OAM

modulated by Fermat-spiral PS and then propagates to the focal plane. Actually, the diffraction field at the focal plane is the coherent superposition of individual diffraction field of each pinhole, which can be calculated by Fresnel-Kirchhoff diffraction formula [13].

$$\mathrm{E}(x,y) = -i\frac{A}{2\lambda}\int_{holes}\frac{e^{ik(r+s)}}{rs}(\cos\delta r + \cos\delta s)dS \tag{1}$$

where E(x,y) is the diffraction field of any given pinhole at the focal plane, A is the amplitude at unit distance from the source and the integral is performed over the pinholes, λ is the incident wavelength, r is the distance from the light source to the given pinhole, s is the distance from the given pinhole to the focal spot, δr is the incident angle between the incident light and the normal of the given pinhole, δs is the diffracted angle between the diffracted light and the normal of the given pinhole. Figure 1b and c indicate the SEM images of Fermat-spiral PS with topological charges of -1 and +3, respectively.

Obviously, the intensity and phase maps of the focused Vortex is determined by the diameter and the position coordinate of each pinhole. Here the Fermat-spiral PS achieves OAM by varying the radial distances of the pinholes with a constant azimuthal increment. In order to determine exactly the position coordinates and the sizes of those transparent pinholes, genetic algorithm is applied to optimize the Fermat-spiral PS [28]. During the optimization process, the unknown parameters R_n, R_n means the radius of the nth ring, and its corresponding pinhole radius a_n. The pinhole number M_n in the ring R_n can be evaluated by $Mn=\frac{2\pi Rn}{ln}$, where l_n is the arc length between the centers of two neighboring pinholes. Taking into account structured

vortex beam in the center surrounded by a series of azimuthally splitting focal spots, in this case a standard Fermat spiral can be chosen as the initial structure to speed up the convergence and improve the design precision of the optical structure. Figure 1d shows the flow chart of the genetic algorithm and Fig. 1e presents the SEM image of Fermat-spiral PS with focused OAM.

Experimental results and discussions

The experimental setup of Fermat-spiral PS focusing is shown in Fig. 2a. The EUV radiation is a capillary discharge 46.9 nm laser with an output energy of 500μJ operating at the single-shot mode [30, 31]. The recording medium, a 200nm thick layer of PMMA (polymethyl methacrylate, 950000 molecular weight) coated on a silicon wafer, is used to record the focal spots and is fixed on a two-dimensional stage to realize z-scan along the beam propagation. Under the condition of single-shot exposure, the energy of the single pulse laser that deposited on PMMA surface is below 1μJ. Each position was exposed by single laser pulse with a dose in the region of the linear response of PMMA. Consequently, the pattern height printed in PMMA surface was equivalent to the focusing light intensity. After the exposure, PMMA was developed by 9 minutes and stopped by 30 seconds, then dried using nitrogen. The processed PMMA targets are detected by atomic force microscopy (AFM).

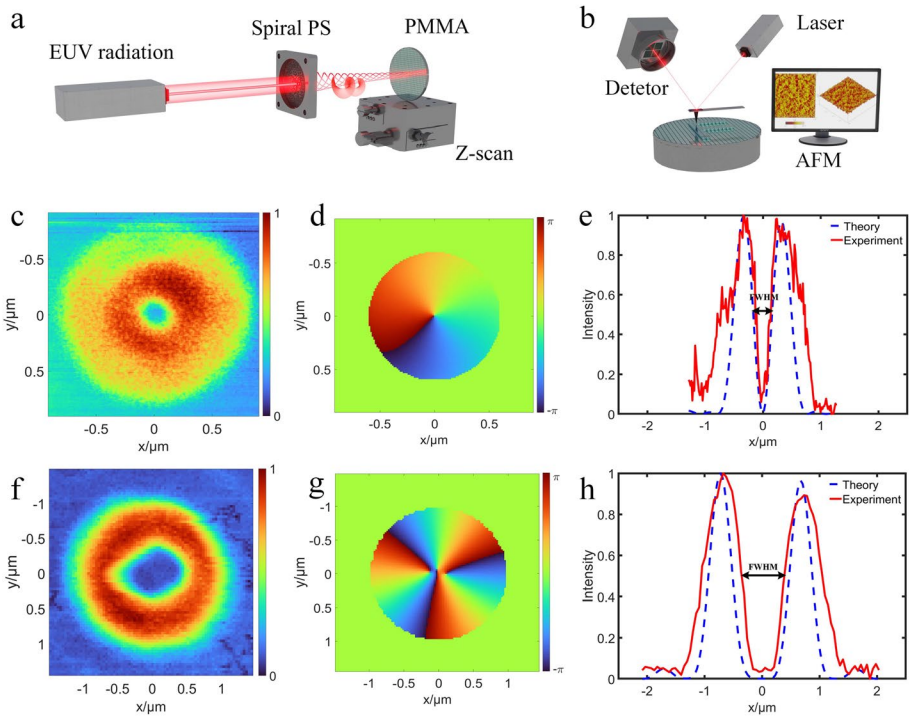

Fig. 2 Sketch of the experiment setup for focused OAM and recorded by PMMA (**a**), detection of AFM (**b**), (**c**) and (**d**) the intensity and phase distribution of the focused OAM with topological charge of -1; **e** diagonal intensity distribution of experimental results versus the theory; **f**, **g** the intensity and phase distribution of the focused OAM with topological charge of +3; **h** diagonal intensity distribution of experimental results versus the theory

To better understand the focused vortex, two Fermat-spiral PSs with topological charge of -1 and +3 are presented and verified by EUV focusing experiment. The corresponding intensity and phase maps of the two foci are separately displayed in the left and middle columns in Fig. 2. Figure 2d and g show the recovered phase map by use of multi-planar coherent diffractive imaging (CDI) [29]. Here, in our experiment configuration, once the three recording distances of diffractogram are obtained, multi-planar CDI is adopted to retrieve the phase information of light field. Concretely, to speed up the convergence rate, the theoretical phase map at the focal plane can be set as the initial guess phase. Therefore, dozens of iterations are enough to reconstruct the wavefront of the object. The details of phase reconstruction process also can be seen in the Supplementary document. Obviously, there is a helical phase in the center of the focused OAM. Figure 2e and h depict the diagonal intensity distributions corresponding to the experimental and theoretical results, respectively. For focused vortices with topological charge of -1 and +3, the experimental results show that the full width at half maximum (FWHM) of the dark ring is 260 nm and 742 nm, respectively. The experimental results indicate that the Fermat-spiral PS can be used to focus the EUV light. The above experimental results demonstrate that our light manipulation on EUV radiation provides opportunities for applications such as nanoscale structure focusing, extreme ultraviolet phase shifters, nano-imaging, and of course, extreme ultraviolet interferometry and diffractometry.

Furthermore, the use of photon sieve offers extremely high degree of freedom in the design to produce more customized focal fields, which may be highly desirable in applications such as nanometer structured lithography, interaction between complex structured light and matter, multichannel particle acceleration and so on. Here, as an example, we demonstrate an anamorphic Fermat spiral to generate focused EUV vortex field dressed with surrounding petals. In this case, we investigated the advantage of using genetic algorithm to optimize the Fermat-spiral PS to produce structured-focusing EUV OAM. Figure 3a-c present three frames of diffractograms from pre- to post-focus position. In order to obtain the real record position in the experiment, correlation coefficient can be calculated via the comparison between the recorded diffractogram and a series of theoretical diffractograms, as shown in Fig. 3d. The centroid corresponding to the maximum correlation coefficient is considered as the real centroid. Thus, the maximum correlation coefficient is 0.94 and the recording distance is plus 5.2 μm derived from the focal plane. Similarly, the maximum correlation coefficient is 0.92 and the recording distance is minus 24 μm derived from the focal plane for Fig. 3a. For Fig. 3c, the maximum correlation coefficient is 0.93 and the recording distance is plus 32 μm derived from the focal plane. Once the record distances are found, multi-planar CDI can be performed to recover the distribution of phase information. Figure 3f shows the recovered phase map corresponding to the square block diagram in Fig. 3e. Obviously, there is also a helical phase in the center. For Fig. 3e, the base width of the dark ring is 467 nm and the base width of the doughnut is about 1.091 μm, while the base width of the dark ring is 428 nm and the base width of the doughnut is 1.013 μm in theory, as shown in Fig. 3g. All details can be seen in the Supplementary ducument.

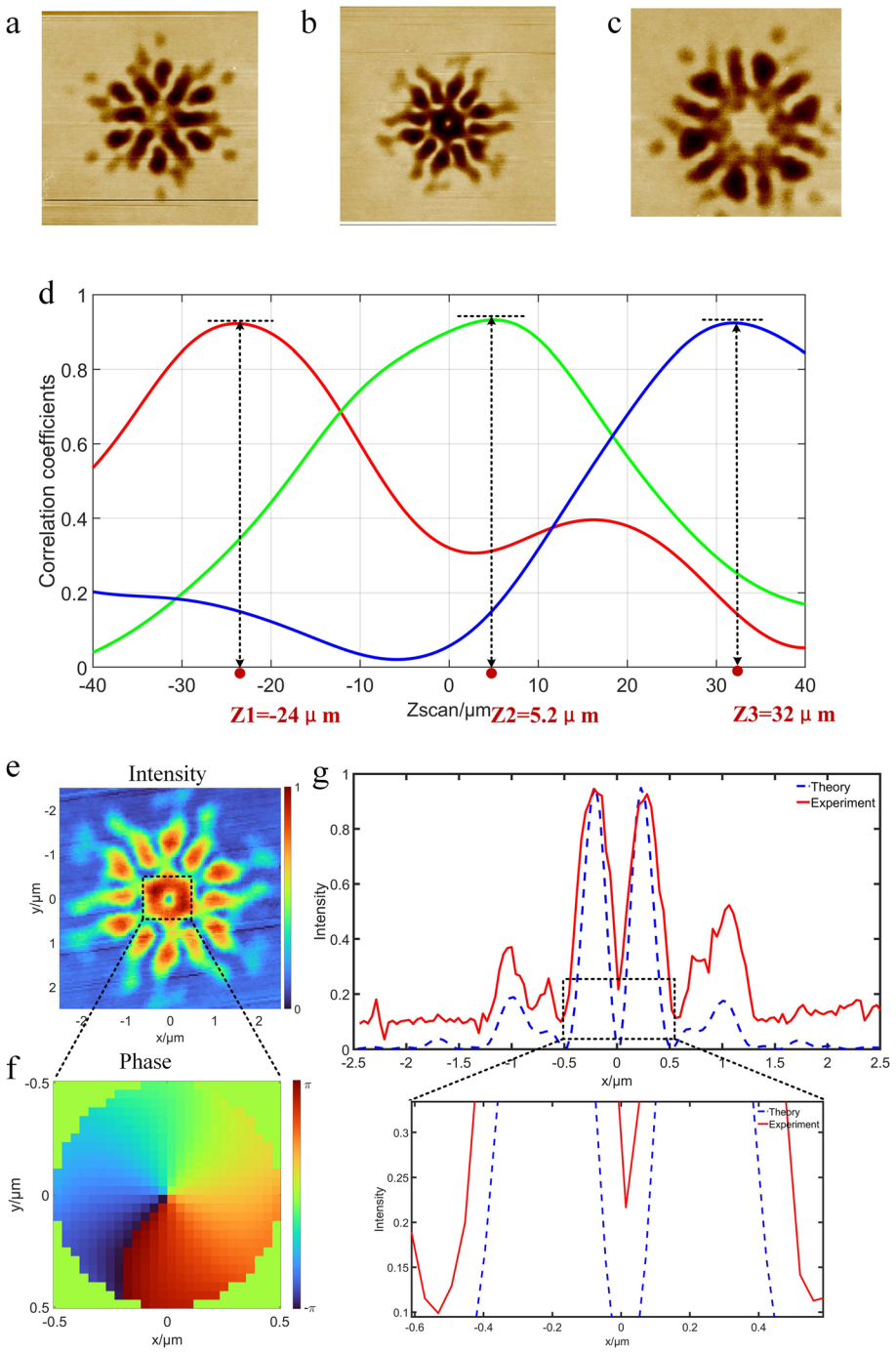

Fig. 3 Experiment on the focused EUV OAM with high degree of freedom, **a** prior to focus, **b** near focus, **c** after focus, **d** Correlation coefficient curve between the (**a**)-(**c**) and a series of theoretical diffractograms from minus 40 μm to plus 40 μm derived from the focal plane, the red line, green line and blue lines correspond to the correlation coefficients curves in (**a**), (**b**) and (**c**), respectively. **f** Recovered phase map corresponds to the square block diagram in (**e**). **g** Diagonal intensity distribution of experimental results versus the theory

Conclusions

In summary, we present the design, fabrication and testing of Fermat-spiral PS for producing focused EUV vortices. The experimental results are in good agreements with the theoretical analysis. The phase distributions of focused EUV vortices with different topological charges are successfully recovered by multi-planar CDI and the central helical phase structures are revealed. Compared with FZP, PS offers several other distinctive advantages. Firstly, PS device can overcome the limitation of spatial resolution determined by the outmost width of the zone. Secondly, compared with the mono-focal FZP, PS with hundreds of thousands of transparent pinholes with different sizes, shapes and position coordinates, offers potential to realize much more complex structured focus such as multi-foci, which may be applied for interferometry and diffractometry in the region of EUV and soft x-ray. Thirdly, the free-standing PS is self-supporting and its fabrication is much easier than supported FZP. Note that as one kind of amplitude-only diffractive element, the diffraction efficiency of the optimized PS is approximately 7%. To further improve the diffraction efficiency, metasurface device [12] may be employed to couple the EUV light to the multifunctional PS. PS with hundreds of thousands of transparent pinholes whose sizes, shapes and position coordinates offers large number of degree of freedom in the design that can be optimized to meet the requirement of various light manipulations ranging from the visible light to EUV and X-rays.

Supplementary Information

The online version contains supplementary material available at https://doi.org/10.1186/s43074-024-00130-x.

Supplementary Material 1.

Acknowledgements
Q.Z.acknowledges support by the Key Project of Westlake Institute for Optoelectronics (Grant No. 2023GD007).

Authors' contributions
J.Z.and Q.Z.conceived and supervised the project. J.Z,H.C.,and Y.Z.designed the optical system. X.Z., Y.Z. and A.Z.analyzed data. Y.L, J.Z. and Q.Z. wrote the manuscript.

Funding
This work has been supported by the National Natural Science Foundation of China (NSFC) (62175245, 62005066, 61875045, 62105345, 62305220 and 92050202), Shanghai Sailing Program (21YF1453700 and 23YF1429300) and Strategic Priority Research Program of Chinese Academy of Sciences (XDA25020302 and XDA25020104).

Availability of data and materials
The datasets used and/or analyzed in the current study are available from the corresponding author upon reasonable request.

Declarations

Ethics approval and consent to participate
There is no ethics issue for this paper.

Consent for publication
All authors agreed to publish this paper.

Competing interests
The authors declare that they have no competing interests.

Received: 2 February 2024 Revised: 27 March 2024 Accepted: 8 April 2024
Published online: 25 April 2024

References

1. Gardner DF, Tanksalvala M, Shanblatt ER, Zhang X, Galloway BR, Porter CL, Karl R Jr, Bevis C, Adams DE, Kapteyn HC, Murnane MM, Mancini GF. Subwavelength coherent imaging of periodic samples using a 13.5nm tabletop high-harmonic light source. Nat Photon. 2017;11(4):259–63.
2. Sivis M, Duwe M, Abel B, Ropers C. Extreme-ultraviolet-light generation in plasmonic nanostructures. Nat Phys. 2013;9(5):304–9.
3. Eschen W, Loetgering L, Schuster V, Klas R, Kirsche A, Berthold L, Steinert M, Pertsch T, Gross H, Krause M, Limpert J, Rothhardt J. Material-specific high-resolution table-top extreme ultraviolet microscopy. Light Sci Appl. 2022;11(1):1–10.
4. Benko C, Allison TK, Cingoz A, Hua L, Labaye F, Yost DC, Ye J. Extreme ultraviolet radiation with coherence time greater than 1s. Nat Photon. 2014;8(7):530–6.
5. Klas R, Demmler S, Tschernajew M, Hadrich S, Shamir Y, Tunnermann A, Rothhardt J, Limpert J. Table-Top Milliwatt-Class Extreme Ultraviolet High Harmonic Light Source. Optica. 2016;3(11):1167–70.
6. Allaria E, Appio R, Badano L, Barletta WA, Bassanese S, Biedron SG, et al. Highly coherent and stable pulses from the FERMI seeded free-electron laser in the extreme ultraviolet. Nat Photon. 2012;6(10):699–704.
7. Rocca JJ, Shlyaptsev V, Tomasel FG, Cortazar OD, Hartshorn D, Chilla JLA. Demonstration of a Discharge Pumped Table-Top Soft-X-Ray Laser. Phys Rev Lett. 1994;73(16):2192–5.
8. Zhao Y, Jiang S, Xie Y, Yang D, Teng S, Chen D, Wang Q. Demonstration of soft x-ray laser of Ne-like Ar at 69.8nm pumped by capillary discharge. Opt Lett. 2011;36(17):3458–60.
9. Géneaux R, Camper A, Auguste T, Gobert O, Caillat J, Taieb R, Ruchon T. Synthesis characterization of attosecond light vortices in the extreme ultraviolet. Nat Commun. 2016;7:12583–1–6.
10. Rego L, San Román J, Picón A, Plaja L, Hernández-García C. Nonperturbative Twist in the Generation of Extreme-Ultraviolet Vortex Beams. Phys Rev Lett. 2016;117(16):163202–1–6.
11. Dorney KM, Rego L, Brooks NJ, San Román J, Liao C-T, Ellis JL, Zusin D, Gentry C, Nguyen QL, Shaw JM, Picón A, Plaja L, Kapteyn HC, Murnane MM, Hernández-García C. Controlling the polarization and vortex charge of attosecond high-harmonic beams via simultaneous spin-orbit momentum conservation. Nat Photon. 2019;13(2):123–30.
12. Ossiander M, Meretska ML, Hampel HK, Lim SWD, Knefz N, Jauk T, Capasso F, Schultze M. Extreme ultraviolet metalens by vacuum guiding. Science. 2023;380(6640):59–63.
13. Kipp L, Skibowski M, Johnson RLM, Berndt R, Adelung R, Harm S, Seemann R. Sharper images by focusing soft Xrays with photon sieves. Nature. 2001;414(6860):184–8.
14. Padgett M, Bowman R. Tweezers with a twist. Nat Photon. 2011;5(6):343–8.
15. Wagner C, Harned N. EUV lithography: Lithography gets extreme. Nat Photon. 2010;4(1):24–6.
16. Shen Y, Wang X, Xie Z, Min C, Fu X, Liu Q, Gong M, Yuan X. Optical vortices 30 years on: OAM manipulation from topological charge to multiple singularities. Light Sci Appl. 2019;8:90–1–29.
17. Hernandez-Garcıa C, Picon A, San Roman J, Plaja L. Attosecond Extreme Ultraviolet Vortices from High-Order Harmonic Generation. Light Sci Appl. 2013;111(8):083602–1–5.
18. Pandey AK, de las Heras A, Larrieu T, San Román J, Serrano J, Plaja L, Baynard E, Pittman M, Dovillaire G, Kazamias S, Hernández-García C, Guilbaud O. Characterization of Extreme-Ultraviolet Vortex Beams with very high topological charge. ACS Photon. 2022;9(3):944–51.
19. Kong F, Zhang C, Bouchard F, Li Z, Brown GG, Ko DH, Hammond TJ, Arissian L, Boyd RW, Karimi E, Corkum PB. Controlling the orbital angular momentum of high harmonic vortices. Nat Commun. 2017;8:14970–1–6.
20. Rego L, Dorney KM, Brooks NJ, Nguyen QL, Liao C-T, San Román J, Couch DE, Liu A, Pisanty E, Lewenstein M, Plaja L, Kapteyn HC, Murnane MM, Hernández-García C. Generation of extreme-ultraviolet beams with time-varying orbital angular momentum. Science. 2019;364(6447):1253–7.
21. Xu S, Ma Y, Zhang J, Zhou S, Zhu J. Multiplanar imaging properties of Fermat-spiral Greek-ladder sieves with different point spread functions. Opt Commun. 2019;434:191–5.
22. Huang Q, Lu X, Zhang H, Wang Z, Yang Y, Zhan Q, Cai Y, Zhao C. Economical generation of high-quality optical vortices with gradual-width Fermat spiral slit mask. Sci China Phys Mech Astron. 2023;66(4):244211–1–9.
23. Ebrahimi H, Sabatyan A. Multi-region spiral photon sieve to produce tailorable multiple vortex. Opt Laser Technol. 2020;126:106137–1–6.
24. Fraczek E, Popiołek-Masajada A, Szczepaniak S. Characterization of the Vortex Beam by Fermat's Spiral. Photonics. 2020;7(4):102–6.
25. Bai Y, Lv H, Fu X, Yang Y. Vortex beam: generation and detection of orbital angular momentum [Invited]. Chin Opt Lett. 2022;20(1):012601–1–15.
26. Yang Y, Thirunavukkarasu G, Babiker M, Yuan J. Orbital-Angular-Momentum Mode Selection by Rotationally Symmetric Superposition of Chiral States with Application to Electron Vortex Beams. Phys Rev Lett. 2017;119(9):094802–1–5.
27. Liu R, Li F, Padgett MJ, Phillips DB. Generalized photon sieves: fine control of complex fields with simple pinhole arrays. Optica. 2015;2(12):1028–36.
28. Huang K, Liu H, Garcia-Vidal FJ, Hong M, Lukyanchuk B, Teng J, Qiu C-W. Ultrahigh-capacity photonic nanosieves operating in visible light. Nat Commun. 2015;6:7059.
29. Pedrini G, Osten W, Zhang Y. Wave-front reconstruction from a sequence of interferograms recorded at different planes. Opt Lett. 2005;30(8):833–5.
30. Zhao Y, Liu T, Zhang W, Li W, Cui H. Demonstration of gain saturation and double-pass amplification of a 69.8nm laser pumped by capillary discharge. Opt Lett. 2016;41(16):3779–82.
31. Zhao Y, Zhao D, An B, Li L, Bai Y, Cui H. Demonstration of double-pass amplification of gain saturated 46.9 nm laser. Opt Commun. 2022;506:127571.

Publisher's Note